New insights on CO and CO_2 hydrogenation for methanol synthesis

The key role of adsorbate-adsorbate interactions on Cu and the highly active MgO-Cu interface

Cao, Ang; Wang, Zhenbin; Li, Hao; Elnabawy, Ahmed O.; Nørskov, Jens K.

Published in:
Journal of Catalysis

Link to article, DOI:
10.1016/j.jcat.2021.06.020

Publication date:
2021

Document Version
Publisher's PDF, also known as Version of record

Journal of Catalysis 400 (2021) 325–331

Contents lists available at ScienceDirect

Journal of Catalysis

journal homepage: www.elsevier.com/locate/jcat

New insights on CO and CO_2 hydrogenation for methanol synthesis: The key role of adsorbate-adsorbate interactions on Cu and the highly active MgO-Cu interface

Ang Cao [a], Zhenbin Wang [a], Hao Li [a], Ahmed O. Elnabawy [a,b], Jens K. Nørskov [a,*]

[a] Center for Catalysis Theory, Department of Physics, Technical University of Denmark, Lyngby 2800, Denmark
[b] Chemical Engineering Department, Faculty of Engineering, Cairo University, Giza 12613, Egypt

ARTICLE INFO

Article history:
Received 20 March 2021
Revised 23 June 2021
Accepted 24 June 2021
Available online 28 June 2021

Keywords:
Methanol synthesis
Density functional theory
Adsorbate-adsorbate interactions
Hydrogen bond
MgO/Cu interface

ABSTRACT

By coupling density functional theory calculations (DFT) with microkinetic modeling, we address two controversial problems pertaining to methanol synthesis: i) Which of the CO or CO_2 hydrogenation routes dominates the synthesis rate, and ii) what makes irreducible, inert oxides like MgO an efficient promoter for the CO hydrogenation process? We determine that the inconsistency between the experimental activity trend and the previous theoretical results in the literature is attributed to the absence of interactions between adsorbed formate and intermediates, which would underestimate the rate of CO_2 route by having a too high formate coverage. We show that when adsorbate-adsorbate interactions, especially the derived H bond, are included, the CO_2 hydrogenation dominates for pure Cu catalysts, which is consistent with experiments. In addition, a new transition state for hydrogenation of adsorbed HCOOH* is discovered, which is further stabilized by hydrogen bonding. We also identify the MgO/Cu interface as a highly active site and propose a novel lattice-oxygen involved reaction mechanism at the interface for methanol formation. The CO hydrogenation reactivity can then be enhanced by stabilizing HCO* in the formate-type species, while the CO_2 hydrogenation is inhibited by the poisoning of CO_2* and HCOO*.

1. Introduction

Commercial methanol synthesis from the CO and CO_2 hydrogenations using Cu-based catalysts is an important industrial catalytic process [1,2]. Despite several decades of research, several issues are still under debate, such as the carbon source (whether CO_2 or CO is the predominant reactant) [3,4], the reaction mechanism [5] and the role of supports [6,7].

Both isotope labeling experiments [3,4] and DFT calculations [8] show that CO_2 is the preferred carbon precursor for methanol formation over ZnO-supported Cu catalysts. This is controversial over un-promoted Cu catalysts. Contrary to early reports [3,9], recent studies [10,11] indicate that CO_2 is preferentially hydrogenated to methanol by comparing the relative activity of the CO and CO_2 hydrogenations. This is also supported by studies on single Cu crystals [12,13], where Cu itself has a little-to-no activity for CO hydrogenation. This, however, is not in agreement with current models based on DFT calculations. For example, Grabow et al. [14] reported a mean-field microkinetic study of the methanol synthesis and RWGS (Reverse Water-Gas Shift) reactions on Cu(111) based on the DFT-determined elementary steps, and found that the CO_2 hydrogenation (i.e., under CO-free feed atmosphere), following the formate mechanism, is less active than CO hydrogenation (i.e., under CO_2-free feed atmosphere), except under the condition of extremely high pressure of hydrogen. A combined experimental and theoretical study reported by Studt et al. [8,15] also showed that whether on the terrace Cu(111) surface or step Cu(211) surfaces, the CO hydrogenation involves intermediates reaction barriers lower in free energy when compared to the CO_2 hydrogenation, thus favoring the CO hydrogenation to methanol.

Distinct from the reducible ZnO promotor, stoichiometric and irreducible MgO is generally believed to be inert to chemical reactions. However, over MgO-supported Cu, the CO hydrogenation was reported to be more active than the CO_2 hydrogenation, which is completely opposite to the experimental result that CO_2 was the carbon source on the unsupported and ZnO supported Cu [10]. Studt et al. [8] also found that even if a low amount of CO_2 is added to the CO/H_2 feed, a clearly decreased methanol synthesis rate is observed on Cu/MgO catalysts. These results indicate that MgO may play a role in switching the preference from the CO_2 hydrogenation to the CO hydrogenation on Cu-based catalysts,

* Corresponding author.
E-mail address: jkno@dtu.dk (J.K. Nørskov).

https://doi.org/10.1016/j.jcat.2021.06.020
0021-9517/

suggesting that it is no longer inert support. Nevertheless, the origin of the MgO support effect on Cu-MgO catalysts for methanol formation is not well understood. Previous reports indicate that metal supports may influence the property of oxide and adsorbates if the oxide is used as a thin film with a few monolayers supported on the metal catalyst, which in turn affects the catalytic activity [16–18]. There are numerous examples where the reactivity of metals is adversely affected when adsorbed on thin MgO films, due to the fact that metals with a rather high electron affinity will become negatively charged, such as MgO grown on Mo, Ag, and Au [19–21]. Therefore, whether the catalytic activity of the CO hydrogenation on Cu can be altered by the Cu-supported MgO film needs to be understood. We believe this question is closely related to that regarding the preference of the CO versus CO_2 hydrogenations towards methanol on Cu-based catalysts.

In this work, we provide a detailed theoretical investigation of these critical issues. Firstly, we studied the activity of CO_2 and CO hydrogenations to methanol formation on Cu(2 1 1). Different from previous theoretical studies, we include adsorbate–adsorbate interactions in our description and show that formate coverage effects and the hydrogen bond formation can significantly lower the activation barrier of the CO_2 hydrogenation, bringing theoretical results in closer agreement with experiments. We further develop a model of the MgO/Cu interface and find the active site at this interface is responsible for the CO hydrogenation. Unlike the reducible ZnO, a lattice-oxygen involved reaction pathway at the Cu-MgO interface for methanol formation is proposed.

2. Computational and modeling methods

DFT calculations were performed using the Vienna *Ab initio* Simulation Package (VASP) [22,23], employing the generalized gradient approximation (GGA) [24] with the van der Waals corrected exchange-correlation functional BEEF-vdW [25] to account for the electron exchange and correlations. Valence electrons were described with the plane-waves with an energy cutoff of 450 eV, whereas core electrons were represented by projector augmented-wave pseudopotentials (PAW) [26].

The stepped Cu(2 1 1) surfaces were modeled as a three-layer (4×3), fcc(2 1 1) slab. The combination of Cu(1 1 1) and MgO (1 0 0) surface was used to model the MgO/Cu interface. The optimized structures of the surfaces are shown in Figs. S4 and S5. All lattice mismatches are less than 4%, which causes strain that is attainable in experiments. The bulk Cu and MgO structures were obtained from the *Materials Project* database [27]. Bulk optimizations were performed for each system before their surfaces were cleaved. Monkhorst-Pack *k*-point meshes of $(2 \times 3 \times 1)$ and $(2 \times 2 \times 1)$ were used to sample the Brillouin zone [28] for the Cu(2 1 1) surface and the models containing MgO, respectively. More than 12 Å of vacuum have been included to separate periodic vertical images. In all the calculations, the bottom layer was fixed at their equilibrium bulk positions, whereas the rest of the layers and the adsorbates were allowed to relax during the geometric optimization until the forces on each atom were less than 0.05 eV/Å.

Transition states (TS) of the reactions were located by the climbing image nudged elastic band (Cl-NEB) method [29] with at least five images generated between the initial and final states. The TS structures obtained by this method were further refined until the forces on atomic centers reach 0.05 eV/Å. Gas-phase energies were corrected using the correction scheme as suggested by Christensen et al. [30], including 0.1 eV per H_2 molecule and 0.29 eV for the CO_2 gas-phase. Zero-point energies and entropic contributions were calculated within the harmonic approximation. Free energy corrections of gas-phase species were obtained using the Shomate equation [31]. The microkinetic modeling was carried out using the CatMAP code [32] based on the mean-field approach and the steady-state approximation.

3. Results and discussion

3.1. Intrinsic activity of Cu(2 1 1) surfaces for CO_2 and CO hydrogenation

In the following, we focus on the Cu(2 1 1) surface as a representative of stepped Cu surfaces, which have been shown to be more reactive for methanol synthesis than Cu terraces [33]. To clarify the reaction mechanism of methanol formation from the CO_2 hydrogenation, a comprehensive study on five widely proposed reaction pathways [34–36] via the reversed water gas shift reaction (RWGS) followed by the CO hydrogenation mechanism and formate mechanism were performed (Fig. S1). As for the RWGS followed by the CO hydrogenation mechanism, CO is found to be a dominant product since the obtained CO* from the RWGS reaction prefers desorption from the surface rather than further hydrogenation to form methanol (Fig. 1a). By comparing the activation energy of different pathways in the formate mechanism (Fig. 1b), the path indicated by the red line is designated to be the most favorable reaction path with the rate-determining step of HCOOH hydrogenation as confirmed by the degree of rate control (Fig. S3). Herein key intermediates are HCOO*, HCOOH*, H_2COOH*, H_2CO*, and CH_3O*, in good agreement with previous works [8,15,37]. For CO hydrogenation, the most efficient paths via HCO*, H_2CO*, and CH_3O* were introduced in this work based on previous work [14,38]. Detailed structures of intermediates and TSs involved in the mechanism of CO_2 and CO hydrogenation are depicted in Fig. S2. The activation energy for methanol synthesis from CO_2 hydrogenation on Cu(2 1 1) is found to be 1.85 eV, which is $\sim$ 0.3 eV higher than that for CO hydrogenation (Fig. 1c). Contrary to the experimental trend, CO_2 hydrogenation is calculated to be roughly three orders of magnitude lower in activity, as shown in Fig. S4.

As an important new feature of this work, we include the effect of adsorbate–adsorbate interaction. Because we noticed that the formate coverage obtained from the microkinetic modeling is close to 1 ML between 500 and 600 K (Fig. 1d, red line), revealing that the surface will be severely poisoned by formate with no more available sites for other intermediates, resulting in a low synthesis rate. We, therefore, focus on the interactions [39] between formate and other intermediates and transition states in the following. To explore the formate coverage on Cu(2 1 1) at experimental conditions, the differential binding energy of HCOO* on the step site was calculated as a function of coverage (Fig. 2a). As shown at the top of Fig. 2a, four different HCOO coverages were introduced, labeled as 0.25, 0.5, 0.75 and 1 ML. The equilibrium coverage of HCOO* is estimated to be $\sim$0.5 ML at 500 K. Even if the reaction temperature rises to 600 K, the step site of Cu(2 1 1) in a unit cell is covered by 2HCOO* (0.5 ML). In experiment, for Cu(1 0 0), Cu (1 1 1) and Cu(1 1 0), the formate saturation coverage are reported in the range from 0.25 ML to 0.33 ML [40–42]. Although no experimental data on Cu(2 1 1) is available, it is rational to presume that the formate saturation coverage is around 0.5 ML since the adsorption energy on stepped Cu211 is stronger than the terraced Cu surfaces. All intermediates and TSs should then be calculated by considering the adsorbate–adsorbate interactions with a pre-adsorbed HCOO*. The calculated reaction paths and the optimized structures of species involved in the CO_2 hydrogenation process are shown in Fig. 3a.

Note that the effect of CO coverage on the activity of CO hydrogenation was not considered in this work. This is because the calculated CO adsorption free energy at low coverage (0.25 ML) is

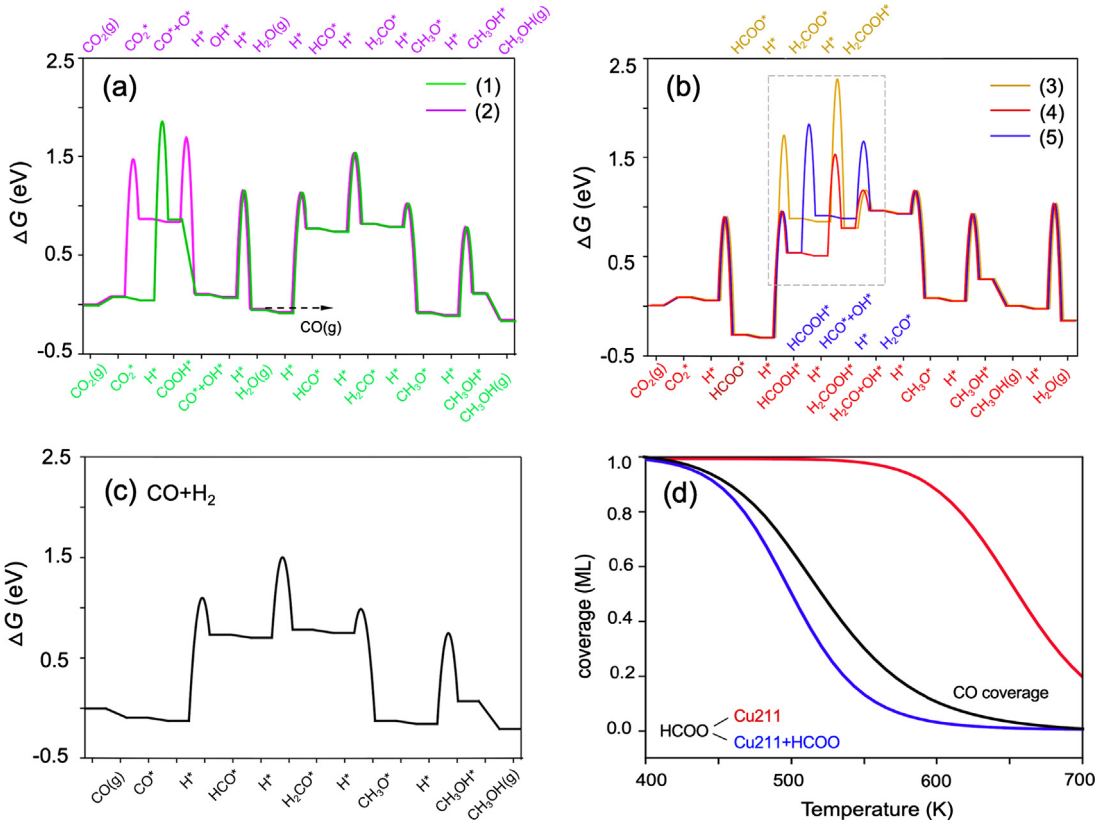

Fig. 1. Free energy diagrams of CO_2 hydrogenation via (a) RWGS followed by CO hydrogenation mechanism and (b) formate reaction mechanism. (c) Free energy diagrams of CO hydrogenation on pristine Cu(2 1 1). (d) Calculated CO* (black line) and HCOO* (red line) coverages using the microkinetic modeling on pristine Cu(2 1 1) and the HCOO* coverage on the surface with a single HCOO spectator (blue line). Free energies of reactants were computed at the temperature of 500 K and a pressure of CO = CO_2 = 10 bar and H_2 = 30 bar; all other free energies were calculated at standard state. (For interpretation of the references to colour in this figure legend, the reader is referred to the web version of this article.)

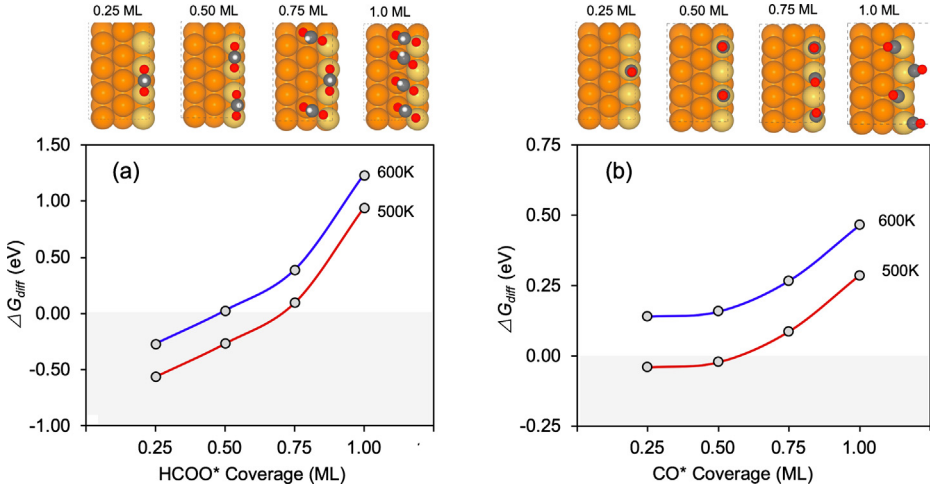

Fig. 2. Coverage-dependent differential binding energies for (a) HCOO* and (b) CO* on Cu(2 1 1). The topmost images depict the configuration of HCOO* and CO* as a function of coverage. Black circles represent energies computed by DFT, and the solid line corresponds to the adsorbate–adsorbate interaction model. Differential binding energies (ΔG_{diff}) are estimated as $\Delta G_{diff} = G(\theta)-G(\theta-0.25)$ for DFT calculations at 500 and 600 K. Adsorption energies of HCOO* are with respect to the gas phase energy of CO_2 (10 bar) and H_2 (30 bar). Adsorption energies of CO are with respect to the energy of CO (10 bar) gas. The shaded region indicates exergonic adsorption. Orange, red, gray, and white spheres represent Cu, O, C, and H, respectively. The Cu atoms on the step sites are labeled in yellow. (For interpretation of the references to colour in this figure legend, the reader is referred to the web version of this article.)

only −0.07 eV at 10 bar CO and T = 500 K, and the adsorption energy becomes weaker with the increase in CO coverage and temperature (Fig. 2b). CO adsorption on Cu(2 1 1) is, therefore, weaker than HCOO adsorption, and CO is not expected to poison the surface at experimental conditions, as confirmed by the low CO coverage obtained from the microkinetic modeling (Fig. 1d, black line).

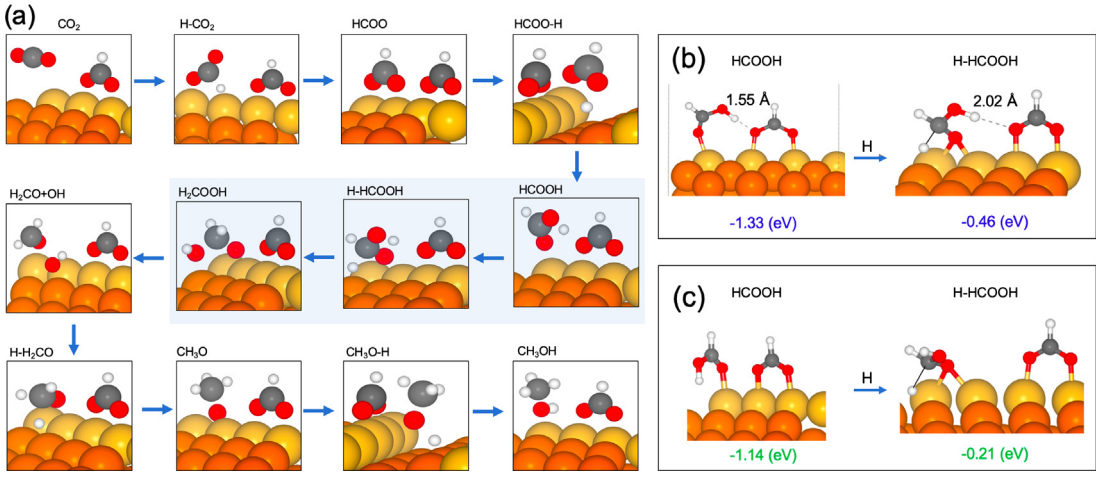

Fig. 3. (a) Reaction paths of CO_2 hydrogenation Cu(2 1 1) with a pre-adsorbed HCOO* species and the optimized structures of intermediates and TSs involved in the reaction. The optimized structures of HCOOH* intermediate and TS of H-HCOOH on HCOO* pre-adsorbed Cu(2 1 1) (b) with and (c) without consideration of H bonding formation. The dashed grey line in (b) represents the H bonding. Orange, red, gray, and white spheres represent Cu, O, C, and H, respectively. The Cu atoms on the step sites are labeled in yellow. (For interpretation of the references to colour in this figure legend, the reader is referred to the web version of this article.)

Another reason is that the adsorption energies of key intermediates involved in CO hydrogenation at the surface with 0.5 ML CO hardly changes compared to the pristine surface (Table S3).

Compared with the pristine surface (Fig. 4a, red line), the adsorption of HCOO* becomes weaker, and the adsorption strength of H-HCOOH* becomes stronger after introducing the HCOO* coverage, which causes the activation energy of the whole reaction to decrease by 0.5 eV (Fig. 4a, blue line). As expected, a significant increase in the methanol formation rate was presented (Fig. 4b, blue line). Meanwhile, the formate coverage obtained from the microkinetic modeling is also significantly reduced (Fig. 1d, blue line). In addition, the methanol formation rate from CO_2 hydrogenation is above 10^{-1} s^{-1} at 500 K, while the rate from CO hydrogenation is two orders of magnitude lower ($\sim 10^{-3}$), showing that CO_2 is preferentially hydrogenated to methanol on pure Cu, in excellent agreement with experimental observations [10].

It is important to note that a new transition state structure of H-HCOOH* with significant hydrogen-bonding stabilization was discovered, as shown in Fig. 3b. Compared to the adsorption structure without an H bond (Fig. 3c), the hydrogen bonding gives rise to a stabilization in the energy of the HCOOH* adsorption and the H-HCOOH* TS of 0.2 eV and 0.25 eV, respectively, which plays a key role in the enhancement of methanol formation rate. Without the formation of the H bond, the activity of CO_2 hydrogenation is still slightly lower than CO hydrogenation, confirmed by the relative methanol formation rate as shown in Fig. S5.

Based on the above analysis, with consideration of interactions between HCOO* and other intermediates, the CO_2 hydrogenation to methanol more favorably proceeds via an H bonding involved formate mechanism on Cu(2 1 1). The high activity of CO_2 hydrogenation on Cu(2 1 1) can be ascribed to the following two reasons. One is the weakened adsorption of HCOO* by considering the realistic HCOO* coverage; The other one is the stabilized H-HCOOH* TS due to the formation of the H bond. Therefore, when adsorbate–adsorbate interactions are included, specifically by the explicit inclusion of spectator HCOO and H bond, the TOFs obtained from microkinetic modeling are in good agreement with experimental results.

3.2. MgO as a promoter in methanol synthesis

To analyze the effects of MgO in CO hydrogenation, here, four different surface models were introduced: Cu supported MgO (MgO/Cu), MgO supported Cu(Cu/MgO), pure Cu(1 1 1) and MgO

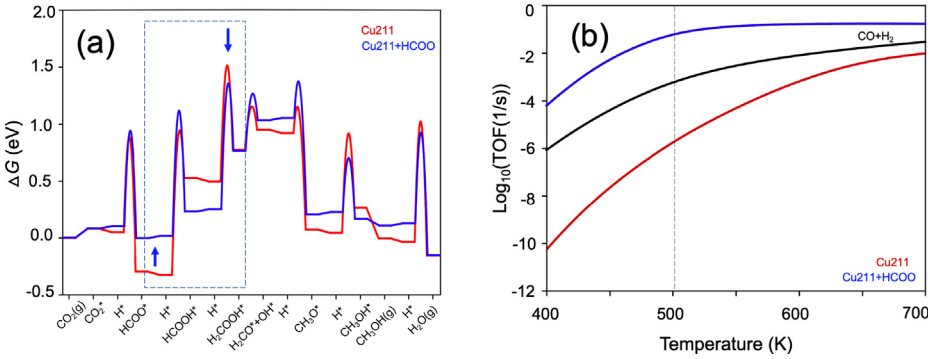

Fig. 4. (a) Free energy diagrams of CO_2 hydrogenation on pristine Cu(2 1 1) (red line) and the surface with one HCOO* adsorbate (blue line). The species added at each step is labeled on the bottom axis. Free energies of reactants are computed at the temperature of 500 K and a pressure of CO = CO_2 = 10 bar and H_2 = 30 bar; all other free energies were computed at standard state. All data used in Figure(a) is listed in Tables S1 and S2. (b) Calculated TOFs using the microkinetic model for methanol formation from CO hydrogenation (black line) and CO_2 hydrogenation on pristine Cu(2 1 1) (red line) on the surface with one HCOO* adsorbate (blue line). The reaction conditions are P_{H2} = 30 bar, P_{CO2} = P_{CO} = 10 bar, and P_{H2O} = P_{CH3OH} ≈ 0 bar. Vertical gray dashed line marks the typical experimental temperature (500 K). (For interpretation of the references to colour in this figure legend, the reader is referred to the web version of this article.)

(100) (Fig. S6). Based on the previously proposed volcano plot for methanol synthesis for CO hydrogenation in Refs. [43,44], we know that a surface with stronger CO* and OH* binding strengths than those of Cu is a prerequisite for developing high-performance catalysts. Therefore, CO* and OH* binding energies on the above four surfaces were calculated (Table S4). There is little change in the binding strengthens of CO* and OH* on pure Cu and the MgO-supported Cu. We, therefore, expect that Cu/MgO has the same low methanol yield as pure Cu. MgO itself is assumed to be inactive due to the extremely weak adsorption of adsorbates. Interestingly, although there is no considerable difference in CO adsorption, the use of Cu support leads to a significant enhancement in the OH* binding strengths on MgO by −1.35 eV.

To explore the origin of the enhanced OH* adsorbate bindings found at the Cu-supported MgO, we calculated the support-induced charge density difference on the systems with adsorbed OH* on the surface (Fig. 5). Fig. 5a shows that for a pristine MgO/Cu surface, the Cu support can induce significant charge redistribution at the interface of Cu and MgO, since the work function of Cu and MgO is 4.65 and 4.94 eV, respectively, benefits the transfer of electrons from Cu to MgO at the interface. When OH is adsorbed on the surface, a considerable charge accumulation can be seen around the adsorbed OH (Fig. 5b), which means the enhancement in the OH* bindings originated from the significant charge transfer from Cu to the adsorbate through MgO. While for CO species, no significant electron transfer was found due to its relatively low electronegativity (Fig. 5c), so the adsorption of CO is not different from that on the pure MgO surface. However, the Cu support acquires an oxidation state after the electrons were transferred, where the oxidation state of Cu can stabilize the adsorption of CO. Based on the fact that both the binding energy of CO and OH needs to be enhanced, we assume that the interface between Cu and MgO is likely to be an active site due to the charge transfer taking place at the oxide/metal interface. At the interface, the adsorption of interfacial OH* can be enhanced by gaining electron charge from Cu via MgO, and the adsorption of CO* can be therefore promoted by the increased oxidation state of Cu sites.

Therefore, a Cu-supported MgO nanorod was modeled to simulate the interface between Cu and MgO (Fig. S7), and a detailed study on the reaction mechanism for CO hydrogenation to methanol was performed at the interface (Fig. 6). As expected, CO prefers to adsorb on the Cu site. The first step of hydrogenation to HCO* then occurs at the boundary of the MgO/Cu interface. While the obtained HCO* species is in a metastable state., which diffuses from the interface to the adjacent MgO surface with a small diffusion barrier of 0.35 eV, and finally combines with the lattice oxygen in MgO by forming a formate-type species. This interesting discovery corroborates recent FT-IR results [10], suggesting that an interfacial formate species is formed in the CO hydrogenation process on Cu-MgO catalysts. The formate mentioned here is composed of the formed HCO* from CO hydrogenation and one lattice oxygen from MgO (denoted as $HCO\_O_{lattice}$). The formed $HCO\_O_{lattice}$ species continues to be hydrogenated to form $H_2CO\_O_{lattice}$ and CH_3O^*. During the formation of CH_3O^*, the H_2CO^* in the TS of H-H_2CO^* would desorb from the lattice oxygen. Thus the lattice oxygen can be released and participate in the reaction of the next cycle. Finally, methanol is formed by the hydrogenation of the obtained CH_3O^* at the MgO/Cu interface.

As shown in the free energy diagram for methanol formation from CO hydrogenation at the MgO/Cu interface (Fig. 7a), the reaction pathway follows $CO^* \rightarrow HCO\_O_{lattice} \rightarrow H_2CO\_O_{lattice} \rightarrow {}^*CH_3O \rightarrow CH_3OH^*$, with the hydrogenation of *CO to HCO* as the rate-determining states. The overall activation energy of CO hydrogenation is 1.2 eV at the interface, which is greater than 0.3 eV lower than that of pristine Cu(211) (Fig. 1c) due to the stronger binding strength of key adsorbates at the interface. For HCO* and H_2CO^* species, the enhanced adsorption energy at the interface could be partially ascribed to the following reasons. One is the charge transfer derived from Cu to the adjacent MgO, where the lattice oxygen can be activated to promote adsorption. The other one is the characteristic adsorption structure of HCO* and H_2CO^* formed by combining with lattice oxygen. For species at the interface that are not bound to the lattice oxygen but bound to the Cu support and an Mg atom simultaneously, such as CH_3O^*, OH*, and CH_3OH^*, the adsorption is enhanced relative to the pristine Cu surface since the adsorbed species at the interface can accept electrons not only from its neighboring Cu atom but also from the distant Cu through MgO.

Meanwhile, the methanol formation rate from CO hydrogenation at MgO/Cu interface and Cu(211) were calculated to be 10^0 and 10^{-3} s^{-1} at 500 K, respectively (red line in Fig. 7c and black line in Fig. 4d). This means that CO hydrogenation is more active at the MgO/Cu interface than at the Cu(211). The MgO/Cu interface is therefore identified to be the active site for CO hydrogenation. Overall, the lattice-oxygen involved reaction pathway of CO hydrogenation is energetically more favorable on the MgO/Cu interface, which shows significantly faster reaction kinetics than the conventional reaction pathway on pure Cu(211) surface.

Why CO_2 hydrogenation is less active than CO hydrogenation on the Cu-MgO catalyst remains unanswered. The blue dashed frame of Fig. 6 shows the reaction paths and the corresponding optimized structures for the intermediates involved in CO_2 hydrogenation. We found that CO_2^* and HCOO* also tend to adsorb on the lattice oxygen to form $CO_{2\_O\ lattice}$ and $HCOO\_{O\ lattice}$ species, which can be confirmed by the detected carbonate/bicarbonate species from FT-IR results [10]. The binding energy of CO_2^* and HCOO* at 500 K was calculated as −0.36 and −0.84 eV, respectively. Such a strong binding strength would poison the surface and lead to a high energy barrier of subsequent reactions. Not surprisingly, it can be seen clearly from Fig. 7b that the activation energy of methanol formation is as high as ~2 eV for CO_2 hydrogenation, which is ~1 eV higher than that of the CO hydrogenation, resulting

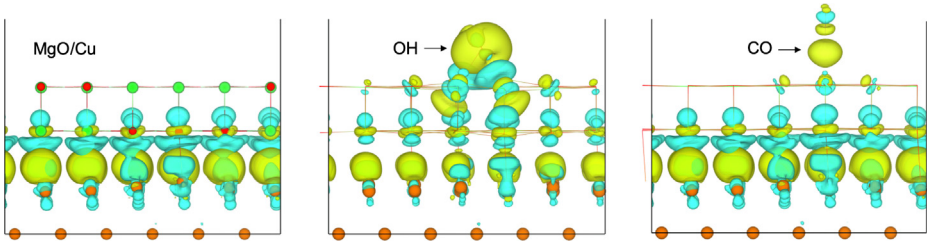

Fig. 5. Calculated charge density difference of the adsorption of CO* and OH* over MgO/Cu(111) surface. Orange, green, and red spheres represent Cu, Mg and O, respectively. The yellow and blue contours represent isosurfaces of charge accumulation and depletion, respectively. The charge density difference was calculated by $\Delta\rho = \rho_1 - \rho_2 - \rho_3 - \rho_4$ (where ρ_1, ρ_2, ρ_3, and ρ_4 represent the charge densities of the whole system, the MgO layer, the Cu(111) support, and the adsorbate, respectively). (For interpretation of the references to colour in this figure legend, the reader is referred to the web version of this article.)

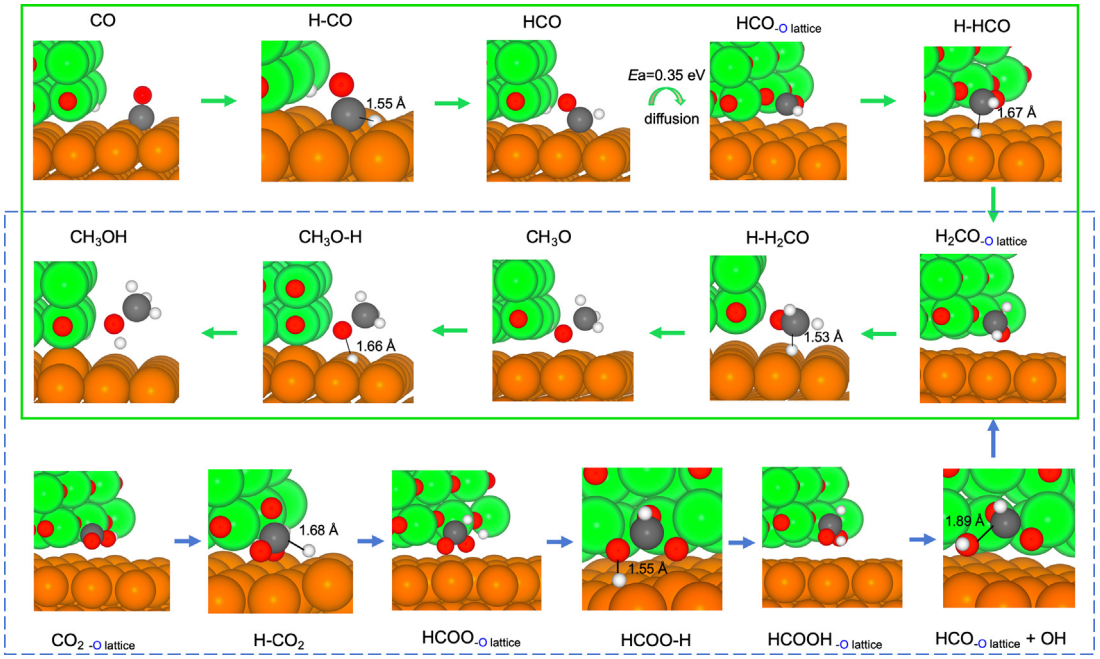

Fig. 6. The most energetically favorable reaction paths for CO hydrogenation (green frame) and CO_2 hydrogenation (blue dashed frame) at the MgO/Cu interface and the optimized structures of intermediates and TSs involved in the two reactions. Orange, green, red, gray, and white spheres represent Cu, Mg, O, C, and H, respectively. (For interpretation of the references to colour in this figure legend, the reader is referred to the web version of this article.)

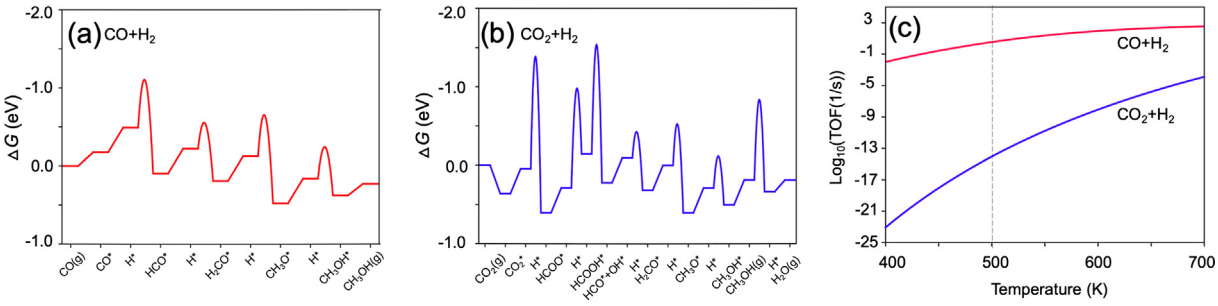

Fig. 7. Free energy diagrams of (a) CO and (b) CO_2 hydrogenation at the MgO/Cu interface. The species added at each step is labeled on the bottom x-axis. Free energies of reactants were computed at the temperature of 500 K and a pressure of CO = CO_2 = 10 bar and H_2 = 30 bar; all other free energies were computed at standard states. (c) Calculated TOFs using the microkinetic model for methanol formation from CO (red line) and CO_2 hydrogenation (blue line) at the MgO/Cu interface. The reaction conditions are P_{H2} = 30 bar, $P_{CO2} = P_{CO}$ = 10 bar, and $P_{H2O} = P_{CH3OH} \approx 0$ bar. The vertical gray dashed line marks the typical experimental temperature (500 K). (For interpretation of the references to colour in this figure legend, the reader is referred to the web version of this article.)

in a rate that is more than ten orders of magnitude lower than that of CO hydrogenation at 500 K (Fig. 7c). Therefore, the CO hydrogenation is dominant on the Cu-MgO catalyst. In addition, the activity towards CO hydrogenation could be strongly inhibited by CO_2 because the formed carbonate/bicarbonate in the CO_2 hydrogenation process occupies the lattice oxygen, and thereby blocking the active site for CO hydrogenation. This is confirmed by the experimental report by Studt et al. [8], where even a low amount of CO_2 present in the CO/H_2 feed significantly lowers the rate of methanol synthesis.

As a result, the MgO/Cu interface is a highly active site for CO hydrogenation, where a lattice-oxygen-involved reaction pathway for methanol formation was first proposed. At the interface, the electron charge is transferred from metal Cu to adsorbates through its adjacent MgO, and the lattice oxygen, therefore, can be activated not only to enhance the adsorption of HCO* but also to reduce the energy barrier of the RDS of CO* hydrogenation to HCO*. While for CO_2 hydrogenation, the poisoning effect by CO_2* and HCOO* at the interface significantly inhibits the activity of this interface towards methanol synthesis.

4. Conclusions

In summary, by combining DFT calculations and microkinetic modeling, we have performed a systematic study on methanol synthesis from CO and CO_2 hydrogenation over pure Cu(2 1 1) and Cu/MgO catalysts and clarified two controversial questions. The following conclusions were reached:

(i) We identified that the reaction path of CO_2 hydrogenation to methanol on un-promoted Cu(211) is: $CO_2 \rightarrow HCOO^* \rightarrow HCOOH^* \rightarrow H_2COOH^* \rightarrow H_2CO^* \rightarrow CH_3OH^* \rightarrow CH_3OH$ (g). But at experimental conditions, the reaction proceeds via hydrogen bond assisted reaction paths, where the formed hydrogen bond plays a key role in stabilizing adsorbate bindings and thus lowering the activation energy.

(ii) The formation rate of methanol on Cu(211) is sensitive to the HCOO* coverage. Only when the interaction between HCOO* and other adsorbates/transition states are included, the results between experiment and theory can be consistent.

(iii) The lattice-oxygen involved reaction pathway of CO hydrogenation is energetically more favorable at the MgO/Cu interface, which leads to significantly faster reaction kinetics than that of the conventional reaction pathway on pure Cu (211). At a MgO/Cu interface, the lattice oxygen in MgO is activated by a significant charge transfer from the Cu support. The CO hydrogenation reactivity then can be enhanced by stabilizing species, while CO_2 hydrogenation is inhibited by the poisoning effect of CO_2* and HCOO*.

We note that since the MgO promotion only takes place at interface while the reducible ZnO wets steps all over the active Cu phase [33,45], the latter is more likely to be an effective promoter due to a higher concentration of active sites. If one could find ways to disperse MgO effectively over Cu or keep Cu particles small on an MgO support,one could increase the efficiency of this promoter significantly.

Declaration of Competing Interest

The authors declare that they have no known competing financial interests or personal relationships that could have appeared to influence the work reported in this paper.

Acknowledgment

Ang Cao thanks Dr. Tao Wang and Dr. Hai Huang (Stanford University), Dr. Ziyun Wang (University of Toronto), Dr. Jakob Munkholt Christensen, and Prof. Ib Chorkendorff (Technical University of Denmark) for their discussions on this work. This project has received funding from the European Research Council (ERC) under the European Union's Horizon 2020 research and innovation program (grant agreement No 741860).

Appendix A. Supplementary material

Supplementary data to this article can be found online at https://doi.org/10.1016/j.jcat.2021.06.020.

References

[1] W. Wang, S. Wang, X. Ma, J. Gong, Chem. Soc. Rev. 40 (2011) 3703–3727.
[2] J. Zhong, X. Yang, Z. Wu, B. Liang, Y. Huang, T. Zhang, Chem. Soc. Rev. 49 (2020) 1385–1413.
[3] L. Uniiiersiiy, Adv. Catal. 31 (1982) 243–313.
[4] G.C. Chinchen, P.J. Denny, D.G. Parker, M.S. Spencer, D.A. Whan, Appl. Catal. 30 (1987) 333–338.
[5] J.A. Rodriguez, P. Liu, D.J. Stacchiola, S. Senanayake, M.G. White, J.G. Chen, ACS Catal. 5 (2015) 6696–6706.
[6] K. Larmier, W.C. Liao, S. Tada, E. Lam, R. Verel, A. Bansode, A. Urakawa, A. Comas-Vives, C. Copéret, Angew. Chemie - Int. Ed. 56 (2017) 2318–2323.
[7] S. Zander, E.L. Kunkes, M.E. Schuster, J. Schumann, G. Weinberg, D. Teschner, N. Jacobsen, R. Schlögl, M. Behrens, Angew. Chemie - Int. Ed. 52 (2013) 6536–6540.
[8] F. Studt, M. Behrens, E.L. Kunkes, N. Thomas, S. Zander, A. Tarasov, J. Schumann, E. Frei, J.B. Varley, F. Abild-Pedersen, J.K. Nørskov, R. Schlögl, ChemCatChem 7 (2015) 1105–1111.
[9] J. Yoshihara, C.T. Campbell, J. Catal. 161 (1996) 776–782.
[10] N.D. Nielsen, J. Thrane, A.D. Jensen, J.M. Christensen, Catal. Lett. 150 (2020) 1427–1433.
[11] N.D. Nielsen, A.D. Jensen, J.M. Christensen, J. Catal. 393 (2021) 324–334.
[12] J. Nerlov, I. Chorkendorff, Catal. Lett. 54 (1998) 171–176.
[13] J. Nerlov, S. Sckerl, J. Wambach, I. Chorkendorff, Appl. Catal. A Gen. 191 (2000) 97–109.
[14] L.C. Grabow, M. Mavrikakis, ACS Catal. 1 (2011) 365–384.
[15] F. Studt, F. Abild-Pedersen, J.B. Varley, J.K. Nørskov, Catal. Lett. 143 (2013) 71–73.
[16] A. Hellman, S. Klacar, H. Grönbeck, J. Am. Chem. Soc. 131 (2009) 16636–16637.
[17] J.D. Baran, H. Grönbeck, A. Hellman, Phys. Rev. Lett. 112 (2014) 1–5.
[18] Y.-N. Sun, L. Giordano, J. Goniakowski, M. Lewandowski, Z.-H. Qin, C. Noguera, S. Shaikhutdinov, G. Pacchioni, H.-J. Freund, Angew. Chemie 122 (2010) 4520–4523.
[19] G. Pacchioni, L. Giordano, M. Baistrocchi, Phys. Rev. Lett. 94 (2005) 8–11.
[20] A. Gonchar, T. Risse, H.J. Freund, L. Giordano, C. Di Valentin, G. Pacchioni, Angew. Chemie - Int. Ed. 50 (2011) 2635–2638.
[21] P. Frondelius, H. Häkkinen, K. Honkala, Phys. Chem. Chem. Phys. 12 (2010) 1483–1492.
[22] G. Kresse, J. Furthmüller, Comput. Mater. Sci. 6 (1996) 15–50.
[23] G. Kresse, J. Hafner, Phys. Rev. B 47 (1993) 558–561.
[24] J.P. Perdew, K. Burke, M. Ernzerhof, Phys. Rev. Lett. 77 (1996) 3865–3868.
[25] J. Wellendorff, K.T. Lundgaard, A. Møgelhøj, V. Petzold, D.D. Landis, J.K. Nørskov, T. Bligaard, K.W. Jacobsen, Phys. Rev. B - Condens. Matter Mater. Phys. 85 (2012) 32–34.
[26] P.E. Blöchl, Phys. Rev. B 50 (1994) 17953–17979.
[27] A. Jain, S.P. Ong, G. Hautier, W. Chen, W.D. Richards, S. Dacek, S. Cholia, D. Gunter, D. Skinner, G. Ceder, K.A. Persson, APL Mater. (2013) 011002.
[28] H. Monkhorst, J. Pack, Phys. Rev. B 13 (1976) 5188–5192.
[29] G. Henkelman, B.P. Uberuaga, H. Jónsson, J. Chem. Phys. 113 (2000) 9901–9904.
[30] R. Christensen, H.A. Hansen, T. Vegge, Catal. Sci. Technol. 5 (2015) 4946–4949.
[31] C.H. Shomate, J. Phys. Chem. 58 (1954) 368–372.
[32] A.J. Medford, C. Shi, M.J. Hoffmann, A.C. Lausche, S.R. Fitzgibbon, T. Bligaard, J. K. Nørskov, Catal. Letters 145 (2015) 794–807.
[33] M. Behrens, F. Studt, I. Kasatkin, S. Kühl, M. Hävecker, F. Abild-Pedersen, S. Zander, F. Girgsdies, P. Kurr, B. L. Kniep, M. Tovar, R. W. Fischer, J. K. Nørskov, R. Schlögl, Science (80-.). 336 (2012) 893–897.
[34] S. Kattel, P.J. Ramírez, J.G. Chen, J.A. Rodriguez, P. Liu, Science (80-.) 355 (2017) 1296–1299.
[35] X. Zhang, J.X. Liu, B. Zijlstra, I.A.W. Filot, Z. Zhou, S. Sun, E.J.M. Hensen, Nano Energy 43 (2018) 200–209.
[36] C. Liu, P. Liu, ACS Catal. 5 (2015) 1004–1012.
[37] F. Studt, I. Sharafutdinov, F. Abild-Pedersen, C.F. Elkjær, J.S. Hummelshøj, S. Dahl, I. Chorkendorff, J.K. Nørskov, Nat. Chem. 6 (2014) 320–324.
[38] Y.M. Liu, J.T. Liu, S.Z. Liu, J. Li, Z.H. Gao, Z.J. Zuo, W. Huang, J. CO2 Util. 20 (2017) 59–65.
[39] N. Yang, A.J. Medford, X. Liu, F. Studt, T. Bligaard, S.F. Bent, J.K. Nørskov, J. Am. Chem. Soc. 138 (2016) 3705–3714.
[40] T. Yatsu, H. Nishimura, T. Fujitani, J. Nakamura, J. Catal. 191 (2000) 423–429.
[41] T. Fujitani, Y. Choi, M. Sano, Y. Kushida, J. Nakamura, J. Phys. Chem. B 104 (2000) 1235–1240.
[42] P.B. Rasmussen, P.M. Holmblad, T. Askgaard, C.V. Ovesen, P. Stoltze, J.K. Nørskov, I. Chorkendorff, Catal. Lett. 26 (1994) 373–381.
[43] J. Schumann, A.J. Medford, J.S. Yoo, Z.J. Zhao, P. Bothra, A. Cao, F. Studt, F. Abild-Pedersen, J.K. Nørskov, ACS Catal. 8 (2018) 3447–3453.
[44] A.J. Medford, A.C. Lausche, F. Abild-Pedersen, B. Temel, N.C. Schjødt, J.K. Nørskov, F. Studt, Top. Catal. 57 (2014) 135–142.
[45] J. Nakamura, T. Fujitani, S. Kuld, S. Helveg, I. Chorkendorff, J. Sehested, Science (80-.). 357 (2017) 1296–1299.